PERGAMON

International Journal of Solids and Structures 39 (2002) 1833–1843

INTERNATIONAL JOURNAL OF SOLIDS and STRUCTURES

www.elsevier.com/locate/ijsolstr

A theory of the densification-induced fragmentation in glasses and ceramics under dynamic compression

Mulalo Doyoyo *

Impact and Crashworthiness Laboratory, Massachusetts Institute of Technology, 77 Massachusetts Avenue, Cambridge, MA 02139-4307, USA

Received 15 May 2001; received in revised form 21 October 2001

Abstract

A boundary of failure which follows a shock front is observed in glasses and ceramics above a critical compressive shock load. This boundary, called the *failure wave* leaves behind a damaged material with newly evolved properties. These include the Tresca yield behavior and the reduction in sound speed. The evolution of the *Mescall zone* during long-rod penetration of these materials is associated with this wave. But, the failure wave and this accompanying process of fragmentation under dynamic compression are still not understood. It is known that some brittle solids undergo an irreversible density increase when subjected to high compression. This phenomenon, called *densification* is linked to the formations of slip lines and cracks in intensely compressed regions of silica glass. It also corresponds directly to the losses in shock wave speeds. Once densified, a region tends to shrink, straining the interface between it and the original solid. Stressed interfaces are unstable and may roughen, causing *local* cracking. On this basis, the failure wave is idealized as a propagating fracture boundary layer where the solid is comminuted by a process of densification interface roughness. The kinetics for this process are established using the fluctuation dissipation theorem. Shear and tensile modes of fragmentation are studied in plane stress. The theory predicts the powder size in the Mescall zone of silica glass. Nevertheless, this theory still needs experimental verification.

Keywords: Silica glass; Ceramic; Failure wave; Dynamic compression; Projectile penetration; Fragmentation; Comminution; Densification; Interface roughness; Mescall zone

1. Introduction

Fragmentation, a process whereby a solid under shock loading breaks into small pieces, involves a number of physical mechanisms that it is difficult to describe. Yet, fragmentation occurs frequently in many impact situations involving brittle solids. Mott explained the fragmentation of metal shells under an impulsive internal pressure using a statistically based fracture criterion (Mott, 1947). Energy balance model by Grady (1988) predicted the size of fragments of a solid subjected to a tensile pulse. A cohesive zone model

* Fax: +1-617-253-1962.
E-mail address: doyoyo@mit.edu (M. Doyoyo).

0020-7683/02/$ - see front matter
PII: S0020-7683(01)00278-5

by Andrews and Kim (1998) described the fragmentation of ceramic particles impacted against a hard steel anvil. These examples show problems where fragmentation is caused by dynamic tension or shear.

Lately, fragmentation under dynamic compression is of great interest in shock physics, but still not well understood. When silica glasses and ceramics are impacted above a certain compressive load, a *failure wave* propagates into the solid leaving behind a damaged material (Brar et al., 1991; Clifton, 1993; Bourne et al., 1998). The damaged medium has a reduced sound speed, and exhibits Tresca yield behavior. Interestingly, during long-rod penetration of silica glass, the Mescall zone (an intensely fragmented medium) is first observed above a dynamic compressive stress of 2.4 GPa (Doyoyo, 2000). The same level of stress is required to generate a failure wave in silica glass. A post-penetration examination shows a clear distinction between the powderized zone and a structurally cracked glass. This powder responds to shock compression as a Mohr–Coulomb material (Klopp and Shockey (1991); Sundaram (1998)).

Also, some brittle solids undergo an irreversible density increase under high quasi-static (Bridgman and Simon, 1953) and shock (Sugiura et al., 1997) compression. This phenomenon called *densification* takes place without altering the tetrahedral Si–O coordination in the glass (Sugiura and Yamadaya, 1992). Thus, the observed permanent decrease on the shock wave speeds corresponds directly to the density increase (Polian and Grimsditch, 1990). Using an indentation test, Hagan (1980) observed the formations of slip lines and cracks in a densified region of silica glass.

Once a region is densified, it will tend to shrink, thereby straining the interface between it and the original solid. The morphology of a stressed interface may change, thus altering the total energy of the system. Particularly, a large change in strain energy will cause morphological instability, which may induce *local* cracking, generating the failure wave. The change in morphology of an interface due to stress is called *stress-induced surface roughness*. This concept has been used to model the evolution of a stress-driven surface roughness in chemical etching (Kim et al., 1999), and the evolution of waviness on the surface of strained thin films (Freund and Jonsdottir, 1993). The driving force for these examples is the chemical potential, and the mechanisms involved are at the atomic level.

Here, the failure wave is idealized as a propagating fracture boundary layer (FBL) behind which fragmentation occurs under dynamic compression. The driving force for the FBL is derived directly from the total energy of the system using the calculus of variations. Conceptually, the FBL represents the limits of stability of each of the solid and comminuted phase forms. Thus, when conditions are favorable (that is, densification interface roughness), the solid phase is unstable and it is comminuted. The governing relation for the process is established using the fluctuation dissipation theorem (FDT) of time-dependent perturbations of a stable interface (Goldenfeld, 1992). Finally, shear and tensile modes of fragmentation are studied in plane stress. The theory also predicts the powder size in the Mescall zone of silica glass.

2. Problem formulation

The schematic of Fig. 1 describes the densification-induced fragmentation in a glass or ceramic during projectile penetration. In the schematic, the projectile penetrates the material at a speed V_p in the X_2 direction. The failure wave or the FBL propagates into the material at a speed V_{FBL} in the same direction. At the same time, the fragments in the Mescall zone are ejected at a speed V_e in the opposite direction. We consider the case when $V_p < V_{FBL}$ at all times t of the penetration event. The enlarged view of the FBL is shown in the schematic. It can be seen that the FBL is a region of transition of length w where a solid phase is transformed into a comminuted phase due to densification interface roughness.

Following Grady (1988), we assume that the role of the local kinetic energy in fragmentation is negligible. This is a strong assumption for a dynamic problem, and the results will be assessed accordingly. Let the densified and original regions be homogeneous, isotropic, linear-elastic solids. If the local strain energy

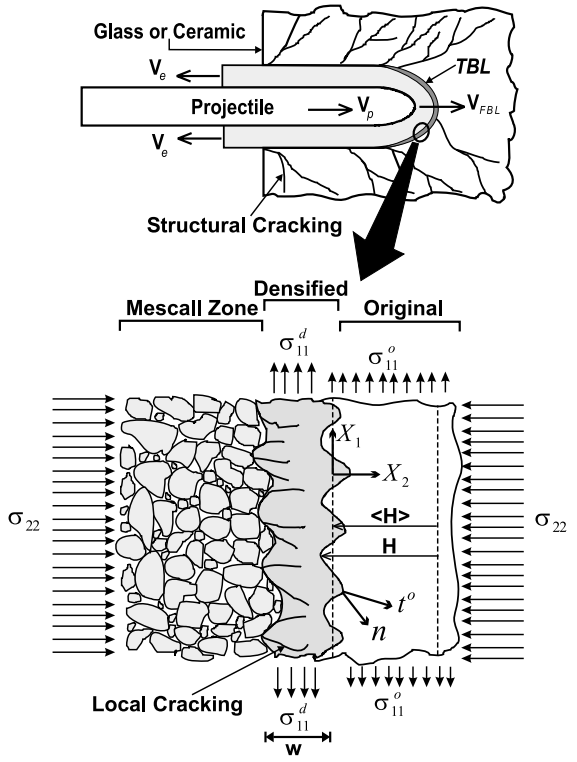

Fig. 1. A schematic of long-rod penetration into a glass or ceramic target. At high dynamic compression, the failure wave comminutes the target by a process of densification interface roughness.

densities in the densified and original materials are denoted by U^{d} and U^{o} respectively, and the interface energy per unit area at the interface is denoted by γ, then the total energy of the system is

$$E = \int_{\Omega^{\mathrm{d}}} U^{\mathrm{d}}\,\mathrm{d}\Omega + \int_{\Omega^{\mathrm{o}}} U^{\mathrm{o}}\,\mathrm{d}\Omega + \int_{S} \gamma\,\mathrm{d}X_1\,\mathrm{d}X_3 \tag{1}$$

where Ω^{d} and Ω^{o} are the volumes of the densified and original regions respectively, and S is the surface area of the interface. X_1 and X_3 are the coordinates parallel to the interface. The interface energy represents the energy of atoms residing in the transition zone. Thus, it may vary across the interface due to changes in the atomic configuration along the interfacial plane. It may also depend on the local strain and strain rates. We will assume that γ is constant. Let t_i^{d} and t_i^{o} represent tractions on the densified and original regions respectively. Further, let the interface be stable in the sense of mechanical equilibrium, so that $t_i^{\mathrm{d}} = t_i^{\mathrm{o}} = t_i$, and let $H(X_1, X_3, t)$ be the height of the interface relative to some reference position. For a stable interface, the *global* minimum of E is obtained by taking the variation of the total energy with respect to H (Courant and Hilbert, 1962). We may call this the energy release rate for the interface, which is

$$L = \int_{S} \left\{ [U] n_2 + t_i \left[\frac{\delta u_i}{\delta H} \right] + \gamma \kappa(H) \right\} \mathrm{d}X_1\,\mathrm{d}X_3 \tag{2}$$

Here, n_2 is the component of the unit normal to the interface along X_2, u_i are the components of the particle displacement and $\kappa(H)$ is the local curvature of the interface. The *square bracket* in Eq. (2) denotes the difference between variables of the original and densified regions (e.g. $[U] = [U^{\mathrm{o}} - U^{\mathrm{d}}]$).

Strains on the interface caused by the tendency of the densified region to shrink can perturb (or *roughen*) the interface. In the presence of a perturbed interface, the condition of mechanical equilibrium at the interface is altered. (An example of the resulting stress state is shown in the schematic of Fig. 1. σ_{22} represents dynamic compression and $\sigma_{11}^{\mathrm{d}} > \sigma_{11}^{\mathrm{o}}$ represents the gain in dynamic lateral tension behind the FBL.) The stresses will roughen the interface, inducing *local* cracking. Suppose the interface is roughened relative to some average height $\langle H \rangle$ such that

$$H = \langle H \rangle + \epsilon h \tag{3}$$

where $\epsilon \ll 1$ and h is the amplitude of the roughness. If the other variables (i.e. tractions, strain energy density, etc.) are similarly perturbed such that Δq represents the perturbed quantity of the variable q, then one can derive part of the energy release rate associated with the perturbation process. If we focus on linear perturbation analysis, we may ignore the terms involving ϵ^2. Recognizing that $\delta u_i/\delta H \sim -\partial u_i/\partial X_2$, then the global energy release rate associated with this roughness process is

$$\Delta L = [\Delta \Gamma] - [\Delta w] \tag{4}$$

where $[\Delta \Gamma]$ and $[\Delta w]$ are the global changes in the interface and strain energies respectively

$$[\Delta \Gamma] = \int_S \gamma \Delta \kappa \, \mathrm{d}X_1 \, \mathrm{d}X_3 \tag{5}$$

$$[\Delta w] = \int_S \left[\sigma_{ij} \Delta u_{i,j}\right] n_2 \, \mathrm{d}X_1 \, \mathrm{d}X_3 \tag{6}$$

Here, σ_{ij} is the Cauchy stress tensor. The local energy release rate ΔL^{l} at some position $\mathbf{X^l} \sim \left(X_1^{\mathrm{l}}, X_3^{\mathrm{l}}\right)$ is evaluated as

$$\Delta L^{\mathrm{l}} = \int_S \Delta L \, \delta\left(\mathbf{X} - \mathbf{X^l}\right) \mathrm{d}X_1 \, \mathrm{d}X_3 \tag{7}$$

where $\delta\left(\mathbf{X} - \mathbf{X}^{\mathrm{l}}\right)$ is the two-dimensional Dirac delta function. The local counterparts of the changes in the interface and strain energies can be similarly evaluated. *We will restrict ourselves to perturbations that are close to equilibrium, or the case* $|\nabla h| \ll 1$. For this case, the change in the local interface energy is given by

$$[\Delta \Gamma]^{\mathrm{l}} \approx \gamma \nabla^2 h \tag{8}$$

where $\nabla^2 = (\partial^2/\partial X_1 + \partial^2/\partial X_3)$ is the two-dimensional Laplacian operator. To obtain the local form of the change in strain energy, we assume that the elastic constants are roughly the same for both the densified and original regions (since densification does not result in significant changes on the basic structural units of the solid). Ignoring *higher-order terms*, the local change in strain energy is given by

$$[\Delta w]^{\mathrm{l}} \approx \int_S \left[\sigma_{ij}\right] G_{ij,k}\left(\mathbf{X} - \mathbf{X^l}\right) [\sigma_{kl}] h_{,l} \, \mathrm{d}X_1 \, \mathrm{d}X_3 \tag{9}$$

for perturbations close to equilibrium. Here, $G_{ij}(\mathbf{X})$ is the interface Green function. The Green function which satisfies the traction and displacement conditions at the densification interface is that of Kelvin's problem (Malvern, 1969), which is

$$G_{ij}(\mathbf{X}) = \frac{1}{16\pi} \frac{1}{\mu_{\mathrm{o}}(1-\nu_{\mathrm{o}})} \left\{ (3 - 4\nu_{\mathrm{o}}) \frac{\delta_{ij}}{r} + \frac{X_i X_j}{r^3} \right\} \tag{10}$$

where $i,j = 1,3$ and $i,j \neq 2$. μ_{o} is the shear modulus of the original material and ν_{o} is its elastic Poisson's ratio. Here, δ_{ij} is the two-dimensional Kronecker delta, and $r^2 = X_1^2 + X_3^2$.

We are now ready to establish the kinetics for the interface roughness process using the FDT. The FDT is used to model the time-dependent fluctuations of a system in equilibrium (Goldenfeld, 1992). For amplitude fluctuations close to the amplitude of the original configuration, the FDT states that "the rate at which the amplitude of the fluctuation relaxes back to equilibrium is proportional to the deviation from equilibrium". If h is the roughness at position $\mathbf{X}^{\mathrm{I}}$, then

$$\frac{\partial h}{\partial t} = -C\Big([\Delta\Gamma]^{\mathrm{I}} - [\Delta w]^{\mathrm{I}}\Big) \tag{11}$$

where C is a phenomenological parameter with the dimensions $\left[\mathrm{L}^{-2}\,\mathrm{M}^{-1}\,\mathrm{T}\right]$, which is assumed to be independent of h. C may be taken as being proportional to the *inverse* of the rate at which a given amount of the original material is densified per unit area. We observe from Eq. (11) that the morphological instability of the interface depends on the dominance of the local change in strain energy over the local change in interface energy. For the interface roughness condition ($\partial h/\partial t > 0$), a high $[\Delta w]^{\mathrm{I}}$ tends to increase the roughness speed, while a high $[\Delta\Gamma]^{\mathrm{I}}$ tends to decrease the speed. Taking a two-dimensional Fourier transform of Eq. (11) with respect to $\mathbf{X}$ and integrating the resulting equation with respect to time t, it can be shown that

$$\ln\frac{\tilde{\boldsymbol{h}}(\omega_i,t)}{\tilde{\boldsymbol{h}}(\omega_i,0)} = \widetilde{C}\left\{\Psi\big([\sigma_{ij}],n_j\big)\omega - \gamma\omega^2\right\} \tag{12}$$

where

$$\Psi\big([\sigma_{ij}],n_j\big) = i\int_{-\infty}^{\infty}\int_{-\infty}^{\infty}[\sigma_{ij}]G_{ij,k}(\mathbf{X})[\sigma_{kl}]n_l\mathrm{e}^{-\mathrm{i}\omega n_m X_m}\,\mathrm{d}X_1\,\mathrm{d}X_3 \tag{13}$$

and

$$\omega_i = \gamma n_i, \quad \omega = \frac{2\pi}{\lambda} \tag{14}$$

In the above equations, the *tilde* denotes the Fourier transformation variables. The parameter ω_i is the component of the wave vector for a given unit normal direction n_i in the interface spectrum. The absolute wave number is represented by ω, while λ is the wavelength of the interface roughness. Here, $\Psi\big([\sigma_{ij}],n_j\big)$ is simplified by first obtaining the Fourier transform of the Green function in Eq. (10) with respect to $\mathbf{X}$, which is

$$\widetilde{G}_{ij}(\mathbf{X}) = \frac{1}{16\pi}\frac{1}{\mu_{\mathrm{o}}(1-\nu_{\mathrm{o}})}\frac{1}{\omega}\left\{4(1-\nu_{\mathrm{o}})\delta_{ij} - n_i n_j\right\} \tag{15}$$

Substituting the above result in Eq. (13) and simplifying the Fourier transform, we get

$$\Psi\big([\sigma_{ij}],n_j\big) = \frac{1}{8\pi}\frac{1}{\mu_{\mathrm{o}}(1-\nu_{\mathrm{o}})}[\sigma_{ij}]\left\{4(1-\nu_{\mathrm{o}})\big(\delta_{ik}n_j + \delta_{jk}n_i\big) - 2n_i n_j n_k\right\}[\sigma_{kl}]n_l \tag{16}$$

Introducing a traction vector, $t_i^* = [\sigma_{ij}]n_j$, and defining $[\sigma_n]$ as a magnitude of t_i^* normal to the interface and $[\sigma_s]$ as a magnitude of t_i^* parallel to the interface, one gets

$$[\sigma_n] = [\sigma_{ij}]n_i n_j \tag{17}$$

and

$$[\sigma_s] = \sqrt{t_i^* t_i^* - [\sigma_n]^2} \tag{18}$$

Writing $\Psi\left(\left[\sigma_{ij}\right], n_j\right)$ in terms of $[\sigma_n]$ and $[\sigma_s]$, we obtain

$$\Psi\left(\left[\sigma_{ij}\right], n_j\right) = \frac{1}{\mu_o}\left\{[\sigma_n]^2 + [\sigma_s]^2 - \frac{1}{4}\frac{1}{1-\nu_o}[\sigma_n]^2\right\} \tag{19}$$

In a Mohr's circle, the point $([\sigma_n], [\sigma_s])$ represents the state of stress jump across the failure wave on a plane with those coordinates. Representing the maximum and minimum stress jumps by $[\sigma_1]$ and $[\sigma_3]$, corresponding to the normal directions n_1 and n_3, then $[\sigma_n]$ and $[\sigma_s]$ can be expressed in terms of these quantities as

$$[\sigma_n] = [\sigma_1]n_1^2 + [\sigma_3]n_3^2 \tag{20}$$

and

$$[\sigma_s] = \sqrt{[\sigma_1]^2 n_1^2 + [\sigma_3]^2 n_3^2 - ([\sigma_1]n_1^2 + [\sigma_3]n_3^2)} \tag{21}$$

Using the above results, $\Psi\left(\left[\sigma_{ij}\right], n_j\right)$ becomes

$$\Psi\left(\left[\sigma_{ij}\right], n_j\right) = \frac{1}{\mu_o}\left\{[\sigma_1]^2 n_1^2 + [\sigma_3]^2 n_3^2 - \frac{1}{4}\frac{1}{1-\nu_o}\left([\sigma_1]n_1^2 + [\sigma_3]n_3^2\right)^2\right\} \tag{22}$$

The size of fragments: At high loads, intersecting slip or flow lines emerge in the densified regions of silica glass below an indenter (Hagan, 1980). These lines represent regions of strain localization, while the material between them deforms elastically. At the kinks, which occur at the intersection points of the flow lines, higher shear displacements and strains are measured. Continued slip on the kinked flow lines can lead to crack nucleation there, followed by crack propagation along the flow lines. Crack interactions, especially in a dynamic environment can comminute the material. The actual process that leads to the formations of the flow lines is not known. Here, we propose that densification interface roughness is such a process. In the same context, we assume that the critical wavelength of the interface roughness is equal to the flow line spacings. *Thus, the critical wavelength of the morphological instability of the densification interface is taken as being of the same order of magnitude as the average fragment size*. The critical wavelength of the densification interface roughness is now presented. One sees from Eq. (12), that the morphology of the interface is unstable if $\gamma\omega^2 < \Psi\left(\left[\sigma_{ij}\right], n_j\right)\omega$. Therefore, there exists a critical wavelength given by

$$\lambda_{cr} = \frac{2\pi\gamma}{\Psi\left(\left[\sigma_{ij}\right], n_j\right)} \tag{23}$$

so that the interface roughness will grow for any $\lambda \geqslant \lambda_{cr}$; otherwise it will decay. According to Eq. (23), the size of fragments is then inversely proportional to the jump in strain energy density across the failure wave.

3. Application in silica glass

In Fig. 1, the failure wave travels in a dynamically compressed brittle solid leaving behind a newly created Mescall zone. This wave was idealized as a propagating FBL where the solid is comminuted by a process of densification interface roughness. Based on this, the size of fragments was shown in Eq. (23) to vary with the inverse of the jump in strain energy across the failure wave. The intention here is to evaluate the fragment size in the Mescall zone of silica glass in plane stress, so that $\sigma_{33} = \sigma_{32} = \sigma_{31} = 0$. Eq. (23) permits us to evaluate fragment size under a combined contribution of shear and tensile stress jumps. Instead, we focus our attention to single-mode fragmentation. We will apply our result to borosilicate, which is a type of silica glass composed of an open silicate network. We shall propose potential scenarios of modes of fragmentation which can be applied to two common shock loading set-ups:

(a) *Shear fragmentation:* As plastic deformation of the bulk occurs according to Tresca flow, the local shear cracking processes are initiated at the flow lines, which eventually comminute the material. This mode of fragmentation is expected to be dominant in a plate-impact test, where the damaged glass or ceramic behind the failure wave exhibits Tresca yield behavior (Bourne et al., 1998). For this mode, the size of fragments is obtained from Eq. (23) as

$$\lambda_{cr} = 2\pi\gamma\mu_o[\sigma_{12}]^{-2} \tag{24}$$

where the jump in the shear stress across the failure wave is given by

$$[\sigma_{12}] = \frac{1-2\nu_o}{2-2\nu_o}\sigma_{22} - k \tag{25}$$

Here, k is the proportional limit in shear. Borosilicate has an elastic Poisson's ratio $\nu_o \sim 0.20$, and shear modulus $\mu_o \sim 31$ GPa. Its shear flow strength behind the failure wave was measured by (Bourne et al., 1998) to be $k \sim 0.90$ GPa. Eq. (25) shows the expected reduction in shear strength behind the failure wave, which is shown diagrammatically in Fig. 2.

(b) *Tensile fragmentation:* Suppression of the Tresca flow after the formation of flow lines could lead to high "lateral tension build-up" in the densified region. Fragmentation is then caused by the local tensile cracking processes. The bulk deforms by a process of sliding and rotation of regions enclosed by the flow lines. This process eventually comminutes the material. This mode of fragmentation is expected during long-rod penetration of brittle solids, where the granulated zone exhibits the Mohr–Coulomb frictional flow (Curran et al., 1993). For this mode, the size of fragments is obtained from Eq. (23) as

$$\lambda_{cr} = 8\pi\gamma\mu_o\frac{(1-\nu_o)}{(3-4\nu_o)}[\sigma_{11}]^{-2} \tag{26}$$

where the jump in the tensile stress across the failure wave is given by

$$[\sigma_{11}] = \left(\frac{\nu_o}{1-\nu_o} - \frac{1-f}{1+f}\right)\sigma_{22} \tag{27}$$

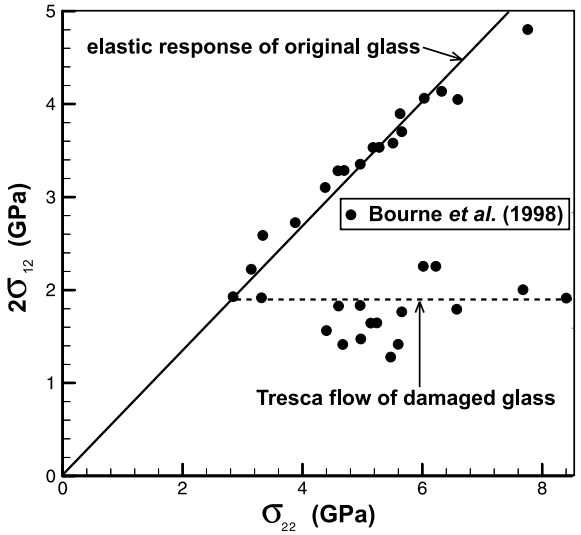

Fig. 2. Reduction in shear strength behind the failure wave (or the FBL) during a plate impact test in borosilicate.

Here, f is the coefficient of internal friction of the Mescall zone, and for borosilicate, it is assumed to be the same as that of ceramic powder, which is $f \sim 0.23$ (Sundaram, 1998). Eq. (27) represents a state of tension "build-up" behind the failure wave, which is shown diagrammatically in Fig. 3.

In the above fragment size equations, the value of the densification interface energy γ of borosilicate is required to complete the calculations. But, this value is not known. The surface energy of borosilicate is about 8 J/m^2. The interface energy of a solid in general lies between the surface energy and zero (DeHoff, 1993). For most compounds, the interface energy is about 0.1–0.2 J/m^2. Yet, densification is a unique type of phase transition in that it does not involve any major structural changes. It is possible that the densification interface energy is slightly higher than the typical interface energies. We shall therefore use several values of the interface energy; $\gamma = 0.1$, 0.2, 0.3 and 0.4 J/m^2.

The size of fragments as a function of dynamic compression for the shear fragmentation mode is shown in Fig. 4, while that of the tensile fragmentation mode is shown in Fig. 5. For the shear mode of fragmentation, the average size of fragments is less than about 0.6 μm. And the average fragment size is less than 0.14 μm for the tensile fragmentation mode. For a given interface energy, the shear mode predicts larger fragments than the tensile mode. In fact, the shear fragments are almost five times bigger than the tensile fragments for the same dynamic compression. Thus, one would expect the powder in the Mescall zone ahead of a long rod to be a lot finer than that in a plate-impact test for similar levels of shock loads. The size of the powder during long-rod penetration of borosilicate was as low as 0.01 μm for dynamic compression as high as 5.2 GPa (Doyoyo, 2000). At 5.2 GPa, the fragments according to the tensile mode of fragmentation range from about 0.01 μm to about 0.03 μm. This comparison is good, but rather indirect. Doyoyo's experiments were performed under axisymmetric conditions. Further, the variation of powder size with dynamic compression was not measured in that investigation. It is also recalled that the contribution of the jump in the local kinetic energy across the failure wave was neglected in the analysis. Indeed, the calculated fragment sizes may be viewed as an *upper bound estimate*!

Comment on the width of the FBL: In the schematic of Fig. 1, the width of the FBL is denoted by w, and the densified material along this width is subjected to lateral tensile stress σ_{11}^{d}. The local cracks are arrested beyond the FBL. According to the Griffith fracture criterion, the cracks will grow to a given length as long as the strain energy is greater than the fracture energy. Applying this criterion to the FBL, one gets

$$w \geqslant \frac{8}{5\pi}\frac{K_{IC}^2}{\sigma_{11}^{\mathrm{d}^2}} \tag{28}$$

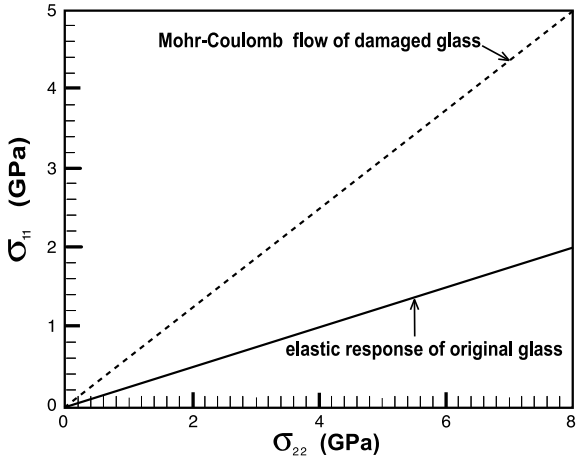

Fig. 3. Lateral tension build-up behind the failure wave (or the FBL) during long-rod penetration of borosilicate.

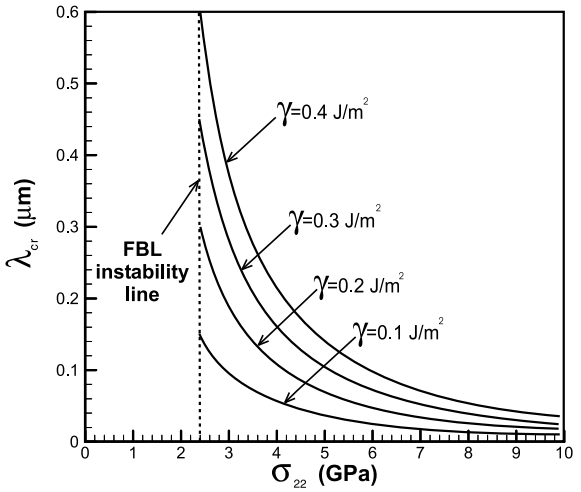

Fig. 4. Dependence of fragment size on dynamic compression for fragments evolved by the shear fragmentation mode in borosilicate.

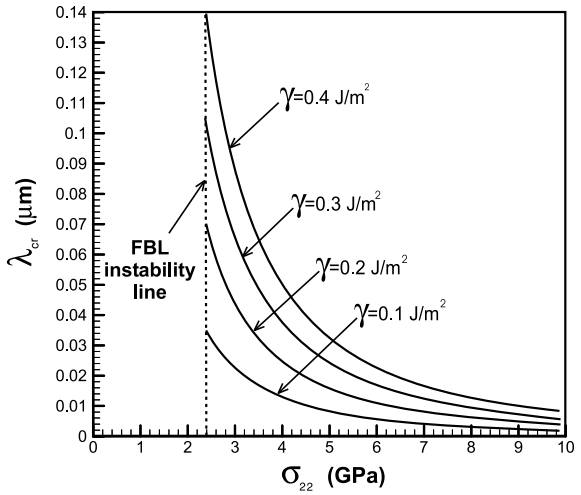

Fig. 5. Dependence of fragment size on dynamic compression for fragments evolved by the tensile fragmentation mode in borosilicate.

for borosilicate. Here, K_{IC} is the fracture toughness which is 0.77 MPa $\sqrt{\text{m}}$ for borosilicate, and σ_{11}^{d} is the lateral tensile stress which is

$$\sigma_{11}^{\text{d}} = \sigma_{22} - 2k \tag{29}$$

for the shear mode of fragmentation, and

$$\sigma_{11}^{\text{d}} = \frac{1-f}{1+f}\sigma_{22} \tag{30}$$

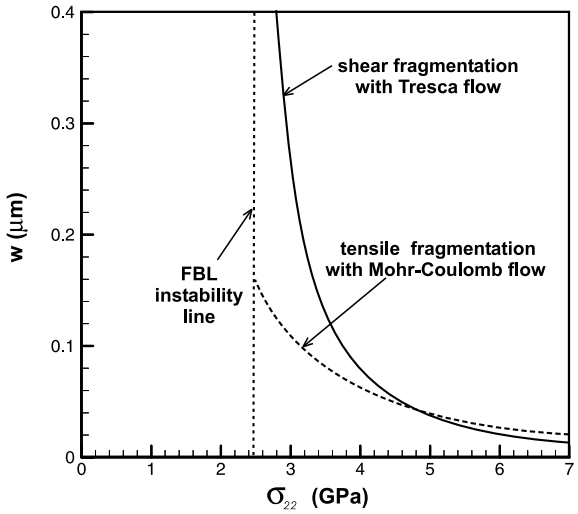

Fig. 6. The effect of dynamic compression on the width of the FBL for shear and tensile fragmentation modes in borosilicate.

for the tensile mode of fragmentation. The variation of the width w with dynamic compression σ_{22} is shown in Fig. 6. It can be seen that the FBL has a submicron width for both fragmentation modes.

4. Conclusion

A theory of the densification-induced fragmentation of glasses and ceramics under dynamic compression has been presented. The theory idealizes the failure wave as a moving FBL where a solid is comminuted by a process of densification interface roughness. The governing relation for this process was established using the FDT of the time-dependent perturbations of a stable interface. Conceptually, when a brittle solid is subjected to high enough dynamic compression, it is densified. The densified region tends to shrink, generating stresses on the interface between it and the original material. This will roughen the interface, which will cause local cracking, creating the failure wave. The size of fragments was shown to be inversely proportional to the jump in the strain energy density across the failure wave. Two modes of fragmentation were proposed for two shock loading configurations: shear fragmentation during plate impact test and tensile fragmentation during long-rod penetration. The shear fragmentation mode predicts about five times bigger fragments than the tensile fragmentation mode. The calculated fragment size for the tensile fragmentation mode compares well with the powder size in the Mescall zone of borosilicate during long-rod penetration. The width of the failure wave was shown to be of submicron size. Further, the jump in the kinetic energy density across the failure wave needs to be included in the analysis. Nevertheless, the physical framework of this theory still needs experimental verification. The theory provides a good basis for future analysis and experiments on the kinetics of the failure wave.

Acknowledgements

It is a pleasure to acknowledge Professor K.-S. Kim of Brown University for numerous useful discussions. I also thank the Brown University Center for Advanced Materials Research for financial support. The Postdoctoral Fellowship from the School of Engineering at MIT is highly appreciated.

References

Andrews, E.W., Kim, K.-S., 1998. Threshold conditions for dynamic fragmentation of ceramic particles. Mech. Mater. 29, 161–180.
Bourne, N.K., Millett, J., Rosenberg, Z., Murray, N., 1998. On the shock induced failure of brittle solids. J. Mech. Phys. Solids 456, 1887–1908.
Brar, N.S., Rosenberg, G.Z., Bless, S.J., 1991. Impact-induced failure waves in glass bars and plates. Appl. Phys. Lett. 59, 3396–3398.
Bridgman, P.W., Simon, I., 1953. Effects of very high pressures on glass. J. Appl. Phys. 24, 405–413.
Clifton, R.J., 1993. Analysis of failure waves in glasses. Appl. Mech. Rev. 48, 540–546.
Courant, R., Hilbert, D., 1962. Methods of Mathematical Physics. Interscience, New York.
Curran, D.R., Seaman, L., Cooper, T., Shockey, D.A., 1993. Micromechanical model for comminution and granular flow of brittle material under high-strain rate application to penetration of ceramic targets. Int. J. Impact Eng. 13, 53–83.
DeHoff, R.T., 1993. Thermodynamics in Material Science. McGraw-Hill, Inc., New York.
Doyoyo, M., 2000. Subsonic projectile penetration into radially confined silica glass cylinders. Ph.D. Thesis, Brown University, Providence, RI.
Freund, L.B., Jonsdottir, F., 1993. Instability of a biaxially stressed thin film on a substrate due to material diffusion over its free-surface. J. Mech. Phys. Solids 41, 1245–1264.
Goldenfeld, N., 1992. Lectures on Phase Transitions and the Renormalization Group Theory. Addison-Wesley, New York.
Grady, D.E., 1988. The spall strength of condensed matter. J. Mech. Phys. Solids 36, 353–384.
Hagan, J.T., 1980. Shear deformation under pyramidal indentation in soda-lime glass. J. Mater. Sci. 15, 1417–1424.
Kim, K.-S., Hurtado, J.A., Tan, H., 1999. Evolution of a surface roughness spectrum caused by stress in nanometer-scale chemical etching. Phys. Rev. Lett. 83, 3872–3875.
Klopp, R.W., Shockey, D.A., 1991. The strength behavior of granulated silicon carbide at high strain rates and confining pressure. J. Appl. Phys. 70, 7318–7326.
Malvern, L.E., 1969. Introduction of the Mechanics of a Continuous Medium. Prentice-Hall, Englewood Cliffs, NJ.
Mott, N.F., 1947. Fragmentation of shell cases. Proc. Roy. Soc. London A 189, 300–308.
Polian, A., Grimsditch, M., 1990. Room temperature densification of silica glass versus pressure. Phys. Rev. B 41, 6086–6087.
Sugiura, H., Yamadaya, T., 1992. Raman-scattering in silica glass in the permanent densification region. J. Non-Crys. Solids 144, 151–158.
Sugiura, H., Ikeda, R., Kondo, K., Yamadaya, T., 1997. Densified silica glass after shock compression. J. Appl. Phys. 81, 1651–1655.
Sundaram, S., 1998. Pressure-shear response of ceramics. Ph.D. Thesis. Brown University, Providence, RI.